RSC Advances

PAPER

View Article Online
View Journal | View Issue

Cite this: *RSC Adv.*, 2025, **15**, 48296

Density functional study of PuC and $PuC_{0.75}O_{0.25}$

Rong Yang, *[a] Zhe Zhang[a] and Bin Tang[b]

We study the structural, magnetic, electronic, thermodynamic and elastic properties of PuC and $PuC_{0.75}O_{0.25}$ using density-functional theory (DFT) and DFT + *U*. The nonmagnetic (NM), ferromagnetic (FM) and antiferromagnetic (AFM) configurations are considered in this work. Total energy results obtained with DFT + *U* indicate that $PuC_{0.75}O_{0.25}$ has an AFM ground state, matching the AFM nature of stoichiometric PuC. Calculated electronic properties reveal a new density of states peak in $PuC_{0.75}O_{0.25}$, a consequence of C/O substitution in PuC. Thermodynamically, $PuC_{0.75}O_{0.25}$ exhibits higher enthalpy difference (H_T–H_{298}), entropy difference (S_T–S_{298}) and heat capacity (C_v and C_p) than PuC at the same temperature; elastically, it is predicted to be harder, owing to the stronger ionic character of Pu–O *versus* Pu–C bonds. Crucially, the formation energy of the oxygen-substitution defect is calculated to be highly spontaneous (−5.11 eV), revealing the fundamental driving force for the oxidation and chemical aging of PuC. These results are intended to provide a valuable reference for further theoretical and experimental investigations of PuC and $PuC_{0.75}O_{0.25}$.

Received 27th August 2025
Accepted 21st November 2025

DOI: 10.1039/d5ra06402c

rsc.li/rsc-advances

1. Introduction

Nuclear energy attracts wide interest owing to its high efficiency, low pollution, and abundant reserves. However, plutonium (Pu), an important nuclear material, slowly reacts with ambient atmospheric components (*e.g.*, O_2, CO, CO_2), forming aging products that impact its long-term stability and performance.[1] Binary products like Pu oxides, hydrides, and carbides have been extensively studied.[2–14] In contrast, investigations into ternary products, such as $PuC_{1-x}O_x$, remain scarce. For $PuC_{1-x}O_x$, experimental observations (*via* XPS)[1,15] and limited theoretical studies (*e.g.*, thermodynamic stability *via* machine learning,[16] lattice constant formulas[17]) have been reported. Critical gaps remain in understanding its fundamental properties: magnetism, thermodynamics and elasticity. These are essential for application assessment. More importantly, the atomic-scale mechanism of aging is unexplored, particularly the role of O-substituted C defects (the most common defect type). Defect formation energy and its correlation with material properties remain unknown.

To address these gaps, this work focuses on $PuC_{1-x}O_x$ (x = 0.25). This composition is selected because it contains a medium amount of oxygen, similar to what forms during early stages of aging. At this stage, the competition between Pu–C and Pu–O bonding becomes very clear. This makes it an ideal model system to reveal the initial effects of oxygen incorporation. We systematically investigate the crystal structure, magnetism, electronic structure, thermodynamic properties, and elastic constants of $PuC_{1-x}O_x$ (x = 0.25). Notably, to clarify the atomic-scale aging mechanism, we calculate the formation energy of oxygen-substituted carbon defects for the first time and correlate it with the material's fundamental properties.

Since Pu is located at a special site where the transition of 5f electrons from itinerancy to localization occurs,[18] it poses a considerable challenge to the theoretical research on $PuC_{1-x}O_x$. In this paper, we use the traditional density functional theory (DFT), DFT plus the Hubbard *U* (DFT + *U*) approach to describe $PuC_{1-x}O_x$. As for the value of U_{eff} parameter, we adopt a value of 4 eV. This value is widely validated in theoretical studies on Pu-based compounds[19–21] for reproducing experimental properties reasonably. We thoroughly discuss the sensitivity of key results to U_{eff} (tested at 3, 4, 5 eV) in the main text, confirming conclusion robustness. Integrating perfect crystal and point defect studies, this work aims to build a fundamental property-aging mechanism correlation for $PuC_{1-x}O_x$, providing theoretical insights for predicting and managing plutonium aging.

The rest of this paper is organized as follows. In Section 2, we give the computational details of this study. In Section 3, we present our results and discussion. First, we validate our method through calculations of the crystal structures and magnetic properties of PuC and $PuC_{0.75}O_{0.25}$. We then report the electronic structures, thermodynamic properties (from 0 to 1000 K), and elastic constants of both systems. Finally, the formation energies of O-substituted C defects in PuC are analyzed. In Section 4, we summarize some general conclusions.

[a]*School of Materials Science and Engineering, Chongqing Jiaotong University, Chongqing 400074, PR China. E-mail: cqyr88@126.com*

[b]*Institute of Finance & Trade, Chongqing City Management College, Chongqing 401331, PR China*

2. Computational details

All calculations are performed using the Vienna *ab initio* simulation package (VASP) version 6.3.0 (ref. 22) code. The exchange–correlation functional is used GGA Perdew–Burke–Ernzerhof (PBE) formalism[23] and the local spin-density approximation (LSDA).[24] These functionals are selected due to their established and widespread application in the first-principles study of plutonium carbides and related compounds.[12–14,20,25] The Hubbard model is used to treat strong correlations within the LSDA + U[26] and PBE + U methods. We set the parameter $U_{eff} = 4$ eV, which is generally used in Pu-based compounds.[19–21] The robustness of key results is tested with U_{eff} values of 3 eV and 5 eV. In the antiferromagnetic (AFM) calculations, we take the $1 - k$ AFM configuration consisting of alternating spin-up and spin-down ferromagnetic sheets along the [100] direction.

We use a $2 \times 2 \times 1$ conventional fcc supercell (containing 4 formula units, 8 atoms) for calculations on the basic bulk properties of PuC and $PuC_{0.75}O_{0.25}$. The key justifications for selecting this supercell are as follows: first, it preserves PuC's intrinsic fcc symmetry, ensuring an accurate representation of bulk material properties without artificial size effects. Second, it allows for the direct modeling of $PuC_{0.75}O_{0.25}$ by replacing one C atom with one O atom, achieving the exact $x = 0.25$ stoichiometry for early-stage oxidation studies. Third, it balances computational cost and accuracy for calculating thermodynamic and elastic properties. For the calculations of defect formation energies in PuC, a larger $2 \times 2 \times 2$ supercell (64 atoms) is used. This larger size reduces spurious interactions between periodic images of the isolated oxygen defect, which is critical for obtaining converged and accurate defect formation energies.

Rigorous convergence tests determine the appropriate plane-wave energy cutoff and k-point meshes, ensuring that total energies are converged to within 1 meV per atom. The results are summarized in Tables 1 and 2. For the 8-atom supercell, a cutoff energy of 500 eV and a $7 \times 7 \times 7$ K-point grid are selected. These settings achieve the following convergence: 0.7 meV per atom (cutoff energy), 0.01 meV per atom (k-point mesh), and ionic forces <0.001 eV Å^{-1}. For the 64-atom defect supercell, a cutoff energy of 400 eV and a $2 \times 2 \times 2$ k-point mesh are sufficient, converging the total energy to within 0.8 meV per atom and 0.3 meV per atom, respectively.

Table 1 Convergence of total energies with respect to the cut-off energy

8-Atom supercell		64-Atom supercell	
Cut-off energy (eV)	$E-E_{600}$ (meV per atom)	Cut-off energy (eV)	$E-E_{500}$ (meV per atom)
300	21	200	23
400	7	300	8
500	0.7	400	0.8
600	0	500	0

Table 2 Convergence of total energies with respect to k-point mesh

8-Atom supercell		64-Atom supercell	
k-Point mesh	$E-E_{8\times8\times8}$ (meV per atom)	k-Point mesh	$E-E_{3\times3\times3}$ (meV per atom)
$5 \times 5 \times 5$	5.38	$1 \times 1 \times 1$	2.5
$6 \times 6 \times 6$	1.31	$2 \times 2 \times 2$	0.3
$7 \times 7 \times 7$	0.01	$3 \times 3 \times 3$	0
$8 \times 8 \times 8$	0	—	—

3. Results and discussion

3.1 Structural and magnetic properties

PuC has a NaCl-type structure, in which the 4a Wyckoff positions are occupied by Pu atoms and the 4b ones by C atoms. The known experimental lattice constant of PuC is 4.965 Å.[27] Experimental works[28,29] indicate that an anti-ferromagnetic transition occurs at 100 K in PuC. Fig. 1 shows the structure of $PuC_{0.75}O_{0.25}$. For the $PuC_{0.75}O_{0.25}$ system, Pu atoms are divided into two categories, as illustrated in Fig. 1. We refer to the Pu atoms near the O atom as Pu_1, and those far away as Pu_2.

The reliability of DFT + U calculation is highly sensitive to the choice of the U_{eff} parameter. To ensure a valid U_{eff} value, we set $U_{eff} = 4$ eV for Pu's 5f orbitals. This choice is justified by theoretical studies on Pu-based compounds,[19–21] which show it reasonably reproduce key experimental properties (*e.g.*, lattice constants, magnetic ordering). To confirm the robustness of our results, we systematically test U_{eff} values of 3, 4 and 5 eV. Details of this analysis, including its impact on the lattice constant (a central structural property), are presented at the end of this section.

Based on the relative total energy values E_{rel} of PuC for the nonmagnetic (NM), ferromagnetic (FM) and antiferromagnetic (AFM) phases given in Table 3, it is evident that the total energies of the FM phase are lower using the LSDA and PBE methods. This suggests that the LSDA and PBE methods predict PuC to be in the FM state, which is not consistent with the available experimental result.[28,29] On the other hand, LSDA + U and PBE + U calculations indicate that PuC is AFM, in

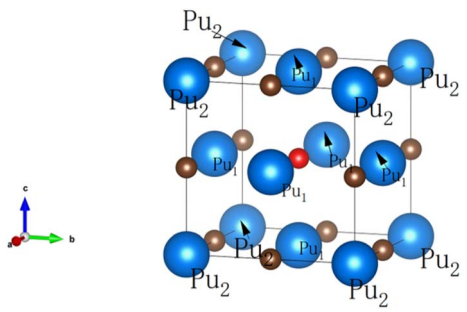

Fig. 1 The crystal structure of $PuC_{0.75}O_{0.25}$. Blue (big) balls represent Pu atoms, brown (small) balls represent C atoms, and red (small) balls represent O atoms. The two distinct Pu sites are labeled: Pu_1 (near O) and Pu_2 (far from O).

Table 3 Compilation of data on nonmagnetic (NM), ferromagnetic (FM) and antiferromagnetic (AFM) states of PuC and $PuC_{0.75}O_{0.25}$: lattice constant (Å), relative energy E_{rel} (eV per PuC/$PuC_{0.75}O_{0.25}$), total magnetic moment μ_{tot} and band gap (eV). The Hubbard parameter U_{eff} is 4.0 eV. Those results are compared to experimental data (ref. 27) and other theoretical values (ref. 16, 17, 20 and 25)

		a_0/Å			μ_{tot}/μ_B			E_{rel} (eV)			E_{gap} (eV)		
Compound	Method	NM	FM	AFM[a]	NM	FM	AFM	NM	FM	AFM	NM	FM	AFM
PuC	LSDA	4.702	4.851	4.847	—	15.730	0.000	2.59	0.00	0.26	0.0	0.0	0.0
	LSDA + U	4.807	4.987	4.976	—	18.023	0.000	17.73	2.44	0.00	0.0	0.0	0.0
	PBE	4.799	4.988	4.984	—	16.481	0.000	4.75	0.00	0.45	0.0	0.0	0.0
	PBE + U	4.916	5.129	5.117	—	18.824	0.000	21.12	3.13	0.00	0.0	0.0	0.0
	Expt.[27]	4.965			—			—			—		
	Ref. 20	—	5.043	5.115	—	17.400	—	—			—	0.0	0.0
	Ref. 25	—	—	4.910	—			—			—		
$PuC_{0.75}O_{0.25}$	LSDA	4.708	4.858	4.854	—	16.606	0.000	2.95	0.00	0.13	0.0	0.0	0.0
	LSDA + U	4.868	5.008	4.987	—	18.701	0.000	14.68	0.26	0.00	0.0	0.0	0.0
	PBE	4.809	4.998	4.991	—	17.478	0.000	5.35	0.00	0.37	0.0	0.0	0.0
	PBE + U	5.037	5.141	5.107	—	18.759	0.000	15.29	0.17	0.00	0.0	0.0	0.0
	Ref. 17	4.968			—			—			—		
	Ref. 16	4.979			—			—			—		

[a] A small tetragonal disorder with $a = b \neq c$ is found in AFM states.

agreement with experiment. The results imply that strong correlation effects exert a significant influence on the magnetism of PuC. Similarly, the LSDA + U and PBE + U methods predict $PuC_{0.75}O_{0.25}$ to be in the AFM state, while the LSDA and PBE methods predict it to be in the FM state. Thus, our results indicate that substituting one oxygen for one carbon does not alter the magnetism in PuC.

As expected, the lattice constant increases when Hubbard U is included. The reason is that the localization of Pu's 5f electrons is enhanced with the introduction of Hubbard U, which weakens the crystal cohesion and thus leads to an increase in the lattice constant. Compared with the experimental data[27] for AFM PuC, the discrepancy is merely 0.22% for LSDA + U but reaches 3.06% for PBE + U. This significant discrepancy demonstrates the superiority of LSDA + U over PBE + U for these materials, as PBE + U overestimates the degree of 5f electron localizations. The fundamental difference stem from how the methods handle electron behavior. LSDA + U maintains a balanced description of electron localization and mobility that matches the actual electronic structure of plutonium compounds. In contrast, the PBE functional inherently overscreens 5f electrons. When combined with the Hubbard U correction, this effect is exaggerated, causing excessive electron localization that weakens atomic bonding and leads to excessively large lattice constants. This advantage of LSDA + U is further confirmed by comparing with other theoretical studies. Table 3 shows that the lattice constant of $PuC_{0.75}O_{0.25}$ predicted by LSDA + U agree well with other theoretical values.[16,17] By contrast, PBE and PBE + U consistently overestimate the lattice constants of PuC and $PuC_{0.75}O_{0.25}$ compared with experimental and theoretical results. This systematic overestimation provides direct evidence that these methods over-localize 5f electrons and underestimate their bonding contributions. Therefore, LSDA + U is more suitable for PuC and $PuC_{0.75}O_{0.25}$ than PBE + U, at least in terms of predicting lattice constants. In both LSDA + U and PBE + U schemes, our calculated lattice constants of FM states are larger than those of AFM states for both PuC and $PuC_{0.75}O_{0.25}$. The optimized lattice constants in AFM states are closer to the experimental or other theoretical values, which suggests that the ground states of PuC and $PuC_{0.75}O_{0.25}$ are likely AFM. Notably, PuC's AFM nature has been confirmed by experimental studies.[28,29]

Of all the methods, LSDA + U yields very accurate lattice constants. For example, for PuC in the AFM state, its calculated value of 4.976 Å deviates from the experimental value by only 0.011 Å. Additionally, when comparing our results with other theoretical values (HSE[20] and SIC-LSD[25]), we find that the lattice parameters obtained by LSDA + U are much better, suggesting that the present method (LSDA + U) has an advantage over the others in describing PuC. For $PuC_{0.75}O_{0.25}$, Ganguly *et al.*[17] provide the lattice constant value of 4.968 Å according to Vegard's law, and R. Z. Qiu *et al.*[16] give a value of 4.979 Å using a machine-learning scheme. Our LSDA + U-calculated lattice constant for the AFM state of $PuC_{0.75}O_{0.25}$ is 4.987 Å, which is close to these results. This suggests that LSDA + U method is also suitable for describing $PuC_{0.75}O_{0.25}$.

In the sequence PuC → $PuC_{0.75}O_{0.25}$, the calculated lattice parameters show an expansion in all methods. For instance, the lattice parameter of $PuC_{0.75}O_{0.25}$ calculated *via* LSDA + U for the AFM state is expanded by 0.011 Å compared to that of PuC. It means that the substitution of carbon atoms by oxygen atoms leads to lattice expansion. The observed lattice expansion has also been reported by Ganguly *et al.*[17] and R. Z. Qiu *et al.*[16]

At the end of this section, Table 4 summarizes the lattice parameters of PuC and $PuC_{0.75}O_{0.25}$ calculated with U_{eff} values of 3.0, 4.0, and 5.0 eV. For PuC, the deviation from experimental data is minimized at 4.0 eV (0.22%), compared to 0.54% at 3.0 eV and 0.60% at 5.0 eV. For $PuC_{0.75}O_{0.25}$, our calculated lattice parameter at 4.0 eV (4.987 Å) is also closest to the previously reported theoretical values.[16] This U_{eff} value is consistent with previous theoretical studies on Pu-based compounds.[19–21] For the oxygen-substituted system, which

Table 4 Lattice parameter of AFM PuC and $PuC_{0.75}O_{0.25}$ calculated using the LSDA + U approach, and comparison to experimental (ref. 27) and theoretical data (ref. 16)

		a_0/Å		
Compound	Method	3.0 eV	4.0 eV	5.0 eV
PuC	LSDA + U	4.938	4.976	4.995
	Expt.[27]	4.965		
$PuC_{0.75}O_{0.25}$	LSDA + U	4.957	4.987	5.007
	Ref. 16	4.979		

lacks experimental lattice data, we further validate $U_{eff} = 4.0$ eV by analyzing the sensitivity of oxygen-induced lattice expansion to U_{eff} variations. The calculated expansion rates are 0.38% at 3.0 eV, 0.22% at 4.0 eV, and 0.24% at 5.0 eV. This low sensitivity confirms that the structural effect of oxygen substitution remains consistent under small changes in U_{eff}, reinforcing the reliability of 4.0 eV. We also compare the performance of different exchange–correlation functionals (PBE, PBE + U, LSDA, and LSDA + U). Only LSDA + U with $U_{eff} = 4.0$ eV reasonably reproduces experimental lattice constants and magnetic ordering for PuC and $PuC_{0.75}O_{0.25}$, while other functionals show significant deviations. Therefore, the LSDA + U method with a U_{eff} parameter of 4.0 eV is employed in all subsequent calculations.

3.2 Electronic properties

The total and partial densities of states for PuC and $PuC_{0.75}O_{0.25}$ in LSDA + U are depicted in Fig. 2 and 3, with all energy scales uniformly referenced to the Fermi level ($E_F = 0$ eV) for direct comparison. Key features (*e.g.*, peak positions, band edges) are labeled explicitly in the figures to clarify their correspondence with electronic states. The total DOS curves of both systems cross E_F with nonzero occupation of Pu 5f electrons. This indicates that both PuC and $PuC_{0.75}O_{0.25}$ are metals, which is in agreement with the calculated band gaps (Table 3). For PuC and $PuC_{0.75}O_{0.25}$, the DOS of Pu atoms is mainly dominated by the 5f partial DOS and the Pu d orbits contribute little to the total DOS. The near-Fermi regions of PuC and $PuC_{0.75}O_{0.25}$ are made up mainly of Pu 5f states, which is similar to the other 5f metal carbides. The experimental valence-band spectra[30] of PuC are characterized by the presence of three sharp peaks within 1 eV, located at the Fermi energy E_F, and at 0.50 and 0.85 eV. We note that our calculated DOS of PuC also has three sharp peaks located at 0.02 eV, 0.36 eV and 0.66 eV.

For PuC, peak A is mainly composed of C 2 s states, and peak B is separated from the following C 2p band by a gap of about 2.64 eV. While for $PuC_{0.75}O_{0.25}$, the band structure of peaks A and B is similar to that of PuC, except for the emergence of a new peak C between them. The new peak is caused by a hybridization between Pu 5f/6d states and O 2p states (Fig. 4). This indicates that the substitution of carbon atoms by oxygen atoms would "break" some Pu–C bonds and "form" some Pu–O bonds. In order to obtain further understanding of the electronic structure and analyze the Pu–O and Pu–C bonds. The difference charge densities along the (010) plane are plotted in Fig. 5. The blue and orange zones represent the loss and the gain of charge. We can observe that the Pu atoms lose charge, the C and O atoms have gained charge. This clearly suggests that there is net charge transfer from the Pu atom to the C and O atom, indicating that the Pu–C and Pu–O bonds have ionic character. The electron transfer observed in the charge density

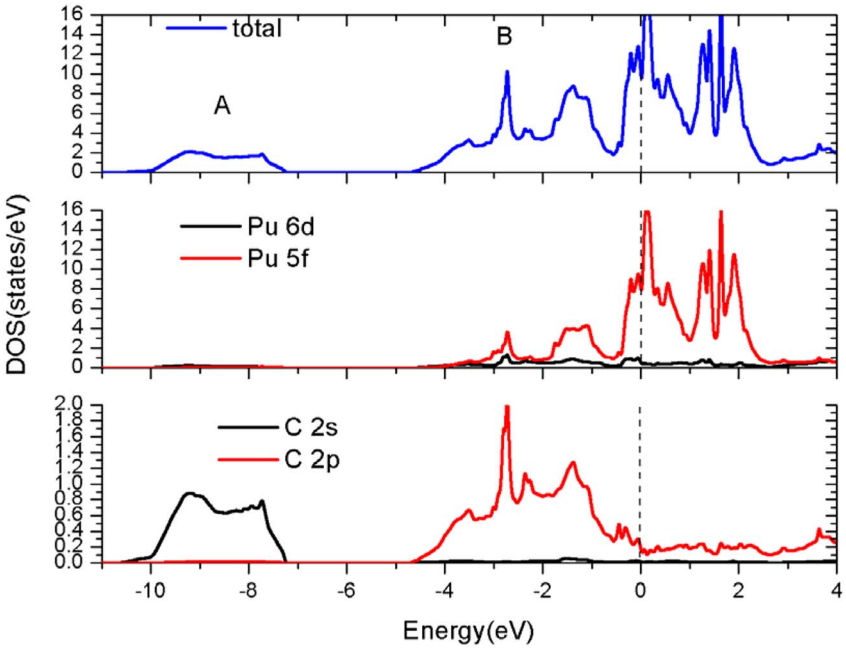

Fig. 2 (Color online) Total and partial densities of states for AFM PuC in LSDA + U ($U_{eff} = 4.0$ eV) framework. The Fermi level is the vertical line through $E = 0$.

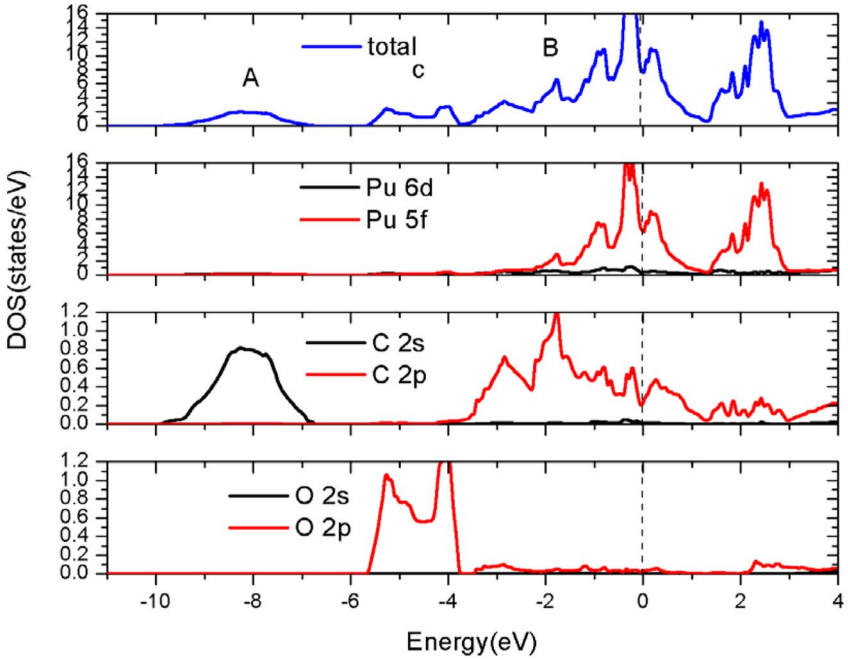

Fig. 3 (Color online) Total and partial densities of states for AFM $PuC_{0.75}O_{0.25}$ in LSDA + U ($U_{eff} = 4.0$ eV) framework. The Fermi level is the vertical line through $E = 0$.

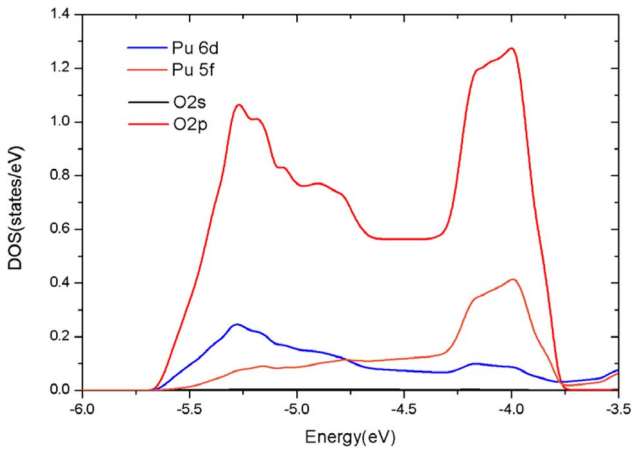

Fig. 4 Partial densities of states for the Pu 6d/5f and O 2s/2p of AFM $PuC_{0.75}O_{0.25}$ in LSDA + U ($U_{eff} = 4.0$ eV) framework.

difference plot is quantified by the Bader charge analysis. As shown in Table 5, each Pu atom loses 1.28|e| and this charge is transferred to C atom in the PuC system. From Fig. 1 and Table 5, in the $PuC_{0.75}O_{0.25}$ system, each Pu atom far from the O atom (Pu_2) still loses 1.28|e| (transferred to the C atom), while each Pu atom near the O atom (Pu_1) loses 1.38|e| (transferred to the O atom). Thus in the $PuC_{0.75}O_{0.25}$ system, the ionic character near the O atom is stronger than that in the PuC system.

For $PuC_{0.75}O_{0.25}$, the crystal symmetry is destroyed with the substitution of carbon atoms by oxygen atoms. Thus, we need to distinguish the partial densities of states (PDOSs) of different C atoms and Pu atoms. To provide an unambiguous description defined by the three-dimensional structure, we label the atoms according to their crystallographic coordinates. We assign the labels Pu1, Pu2, Pu3, and Pu4 to the four plutonium atoms at coordinates (0, 0, 0), (0, 0.5, 0.5), (0.5, 0, 0.5), and (0.5, 0.5, 0), respectively. As shown in Fig. 6, the 6d PDOSs of different Pu atoms are similar, while the two main peaks of 5f PDOSs of Pu1 and Pu2 are further separated than those of Pu3 and Pu4. The near-Fermi regions of total DOS are dominated by the 5f PDOS of Pu_3 and Pu_4. Fig. 7 shows that the 2s and 2p PDOSs of different C atoms are similar.

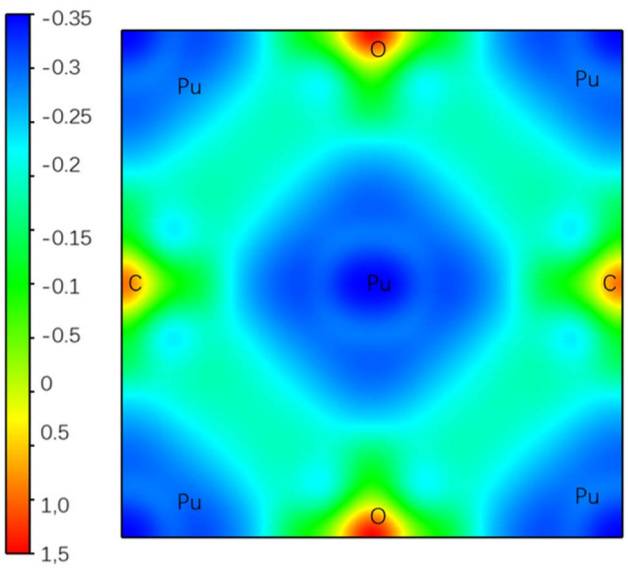

Fig. 5 Contour plots of charge density difference along the (010) plane in LSDA + U ($U_{eff} = 4.0$ eV) calculations of AFM $PuC_{0.75}O_{0.25}$.

Table 5 Calculated Bader charges (Q_B) and Bader volumes (V_B) for AFM PuC and AFM $PuC_{0.75}O_{0.25}$ in LSDA + U (U_{eff} = 4.0 eV) framework

Compound	Q_B (Pu_2)/e	Q_B (Pu_1)/e	Q_B (C)/e	Q_B (O)/e	V_B (Pu_2)/Å^3	V_B (Pu_1)/Å^3	V_B (C)/Å^3	V_B (O)/Å^3
PuC	14.72	—	5.28	—	19.77	—	12.89	—
$PuC_{0.75}O_{0.25}$	14.72	14.62	5.28	7.38	18.92	18.66	12.83	11.81

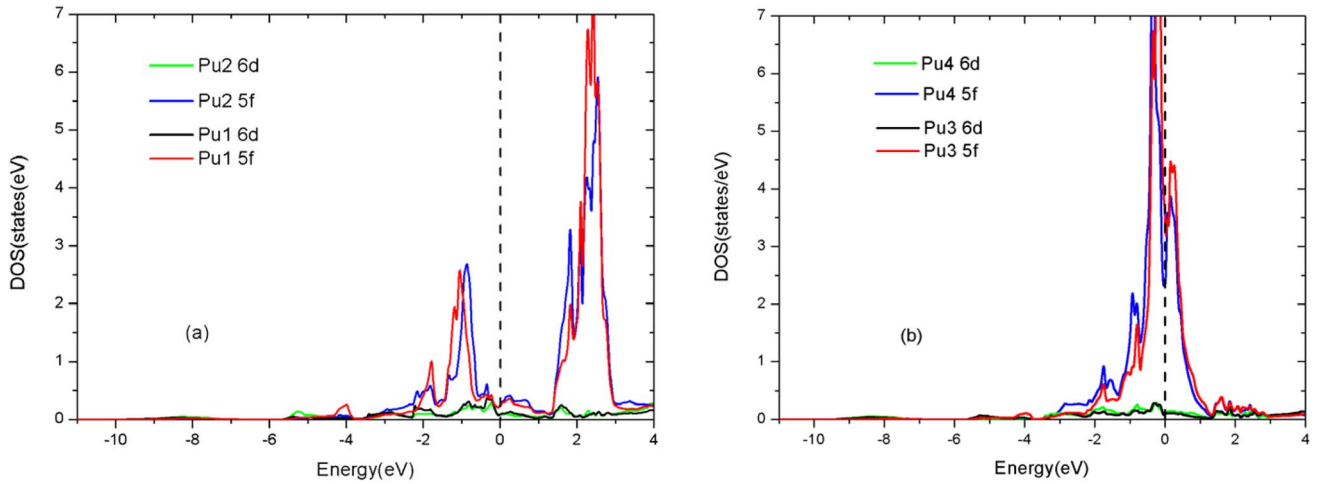

Fig. 6 (Color online) site-projected densities of states of AFM $PuC_{0.75}O_{0.25}$ for different Pu atoms in LSDA + U (U_{eff} = 4.0 eV) framework. (a) Pu1 (0, 0, 0) and Pu2 (0, 0.5, 0.5); (b) Pu3 (0.5, 0, 0.5) and Pu4 (0.5, 0.5, 0). The Fermi level is the vertical line through $E = 0$.

3.3 Thermodynamic properties

For fuel materials, a thorough understanding of their thermodynamic properties is of particular importance. However, available thermodynamic data for plutonium carbides have significant uncertainty due to insufficient experimental data.[31] The thermodynamic properties of PuC and $PuC_{0.75}O_{0.25}$ are investigated herein using phonon density of states obtained *via* the quasiharmonic approximation (QHA).[32] The internal energy ΔE, Helmholtz free energy ΔF, entropy S, and constant-volume specific heat capacity C_v are given, respectively, by[33]

$$\Delta E = 2nN\frac{\hbar}{2}\int_0^{w_L} w\coth\left(\frac{\hbar w}{2k_BT}\right)g(w)\mathrm{d}(w) \quad (1)$$

$$\Delta F = 3nNk_BT\int_0^{\infty}\ln\left\{2\sinh\left(\frac{\hbar w}{2k_BT}\right)\right\}g(w)\mathrm{d}(w) \quad (2)$$

$$S = 3nN\frac{\hbar}{2}\int_0^{w_L}\left[\frac{\hbar w}{2k_BT}\coth\frac{\hbar w}{2k_BT} - \ln\left\{2\sinh\left(\frac{\hbar w}{2k_BT}\right)\right\}\right]g(w)\mathrm{d}(w) \quad (3)$$

$$C_v = 3nN\frac{\hbar}{2}\int_0^{w_L}\left(\frac{\hbar w}{2k_BT}\right)^2\mathrm{csch}^2\left(\frac{\hbar w}{2k_BT}\right)g(w)\mathrm{d}(w) \quad (4)$$

where w is the phonon frequency, $g(w)$ is the normalized phonon DOS, N is the number of unit cells, k_B is the Boltzmann constant and $\hbar$ is the reduced Planck constant. The enthalpy change is expressed by the equation:[34] $\Delta H = \Delta E + P\Delta V$, where E denotes internal energy, P is pressure and V represents volume. For solid and liquid phases, the $P\Delta V$ term is negligible in comparison to ΔE. Moreover, with the equilibrium pressure set to zero, it follows that $\Delta H \approx \Delta E$.

The enthalpy changes (H_T–H_{298}) with increasing temperature are presented in Table 6. For PuC, our calculated values are in good agreement with experimental data.[35] However, a notable temperature-dependent deviation exists. At 427.6 K, the calculated value is 7% higher than the experimental value, whereas it is 7% lower at 921.7 K. This reverse discrepancy is primarily attributed to the inherent limitations of the QHA, particularly its neglect of electronic thermal contributions and anharmonic phonon effects.[36] At a moderate temperature like 427.6 K, the overestimation arises mainly because the model fails to fully reproduce the finite-temperature amplitudes of low-frequency phonons within its T = 0 K harmonic framework. Additionally, the neglect of electronic excitations, though minor, plays a non-negligible role. At 921.7 K, the underestimation is dominated by significant anharmonic effects such as phonon–phonon scattering, beyond the scope of the QHA framework. Thus, it is the temperature-induced emergence of these anharmonic processes that drives the observed breakdown. The deviation is further increased by the growing importance of omitted electronic contributions and higher-order anharmonic effects at high temperature. Volume effects from thermal expansion also contribute to the overall error, but their role is secondary to the effects previously described. Table 6 also lists our calculated values of $PuC_{0.75}O_{0.25}$ at selected temperatures. Specifically, oxygen substitution in PuC leads to a greater enthalpy difference (H_T–H_{298}) at the same temperature relative to pure PuC. This phenomenon can be explained using fundamental thermodynamic relationships: $H_T - H_{298} = \int_{298K}^{T} C_p(T')\mathrm{d}T'$. Since H_T–H_{298} is the integral

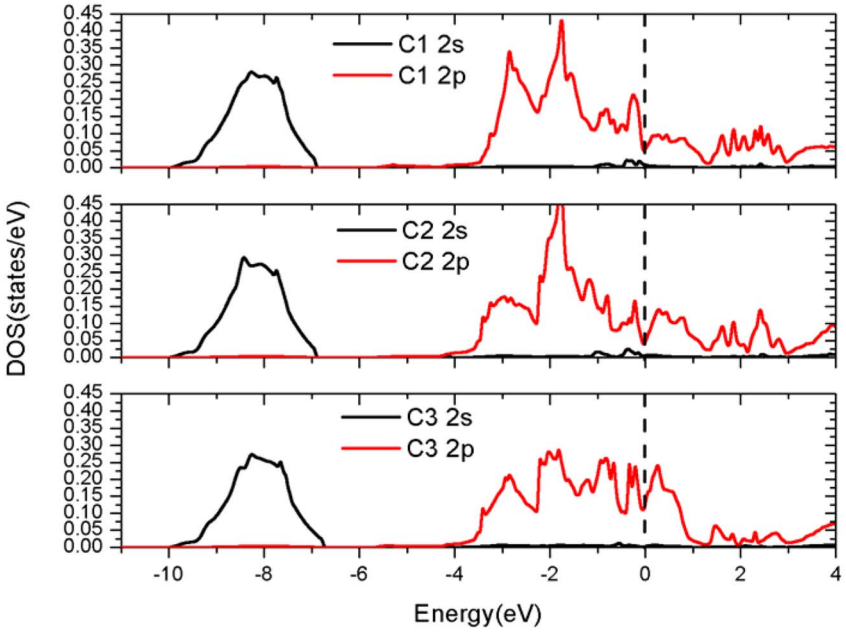

Fig. 7 (Color online) Partial densities of states of AFM $PuC_{0.75}O_{0.25}$ for different C atoms in LSDA + U (U_{eff} = 4.0 eV) framework. The Fermi level is the vertical line through E = 0.

Table 6 Our calculated H_T–H_{298} (kJ mol^{-1}) of PuC and $PuC_{0.75}O_{0.25}$ in LSDA + U (U_{eff} = 4.0 eV) framework, along with the corresponding experimental data (ref. 34)

Compound	Method	425.2 K	427.6 K	525.2 K	530.1 K	628.0 K	733.2 K	825.2 K	830.5 K	921.7 K
PuC	LSDA + U	6.075	6.183	10.940	11.171	15.970	21.175	25.715	25.991	30.520
	Expt.[34]	5.990	5.745	11.054	11.006	16.460	22.108	28.049	27.416	32.626
$PuC_{0.75}O_{0.25}$	LSDA + U	6.999	7.110	11.826	12.032	16.844	22.786	26.631	26.858	31.425

of C_p, and oxygen substitution increases C_p (as shown in Table 7), the H_T–H_{298} of $PuC_{0.75}O_{0.25}$ is therefore more significant than that of pure PuC at the same temperature.

Table 7 presents our calculated values of S_T–S_{298} (J K^{-1} mol^{-1}) and heat capacity (J K^{-1} mol^{-1}) for PuC and $PuC_{0.75}O_{0.25}$ using the QHA. Kruger and Savage[35] calculated the constant-pressure specific heat capacity (C_p) of PuC using the equation (C_p = 13.08 + 11.44 × 10^{-4}T − 3.232 × 10$^5T^{-2}$) proposed by Maier and Kelley.[37] The relationship between C_p and C_v is given by the following equation:[38]

$$C_p = C_v + T\left(\frac{\partial V}{\partial T}\right)_p \left(\frac{\partial P}{\partial T}\right)_V \Big|_{V=V_0(T)} = C_v + \partial^2 BVT \qquad (5)$$

where α denotes the volume thermal expansion coefficient, B is the bulk modulus, V represents the volume, and T is the absolute temperature. From Table 7, the entropy difference S_T–S_{298} calculated in this work can also be compared with other theoretical results.[35] In terms of heat capacity, the agreement between our calculations and the data from Kruger and Savage[35] is not as good as that observed for S_T–S_{298}. Beyond the limitations of the QHA, our calculations only account for vibration entropy (derived from phonon modes) and neglect the electronic contribution to entropy. This oversight leads to a growing discrepancy between our results and Kruger and Savage's data[35] as temperature increases. Furthermore, as indicated by eqn (5), the C_v values differ from the C_p values, with the difference becoming more pronounced at high temperature. At high temperature (over 800 K), our calculated C_v for PuC tends to a constant value of 49.6 J K^{-1} mol^{-1}, which is very close to the Dulong–Petit limit. The Dulong–Petit law[39] states that $C_v = 3N \times R$, where N is the number of atoms per formula unit and R is the gas constant. For PuC, each formula unit contains two atoms, giving a theoretical value of 49.9 J K^{-1} mol^{-1}. Notably, the deviation between our calculated value and this theoretical limit is only 0.6%. The C_v of $PuC_{0.75}O_{0.25}$ also approaches the classical limit (49.9 J K^{-1} mol^{-1}) at high temperatures, as expected from the Debye model. At the low temperature, our calculated C_v for $PuC_{0.75}O_{0.25}$ is higher than that of pure PuC. Local lattice distortions from oxygen substitution are responsible for the enhancement. They generate additional defect vibrations that the standard Debye model does not capture. The increase in entropy similarly stems from the structural disorder induced by these point defects. To quantitatively understand these thermal properties, the Debye temperatures (θ_D) of PuC and $PuC_{0.75}O_{0.25}$ are derived from the phonon DOS. Fitting the DOS to the Debye model ($g_D(w) = 9\,Nw^2/w_D^3$ for $\omega \leq \omega_D$) gives θ_D

Table 7 Our calculated S_T–S_{298} (J K^{-1} mol^{-1}) and heat capacity (J K^{-1} mol^{-1}) of PuC and $PuC_{0.75}O_{0.25}$ in LSDA + U (U_{eff} = 4.0 eV) framework, along with other theoretical values (ref. 34)

		S_T–S_{298} (J K^{-1} mol^{-1})		Heat capacity (J K^{-1} mol^{-1})	
Compound	T (K)	LSDA + U	Other[34]	C_v (LSDA + U)	C_p (other)[34]
PuC	400	13.622	13.209	48.177	48.154
	500	24.451	24.369	48.785	51.665
	600	33.377	24.369	49.163	53.797
	700	41.025	42.427	49.397	55.260
	800	47.681	49.909	49.481	56.388
	900	53.462	56.514	49.572	57.308
	1000	58.816	62.742	49.624	58.102
$PuC_{0.75}O_{0.25}$	400	14.047	—	48.459	—
	500	24.938	—	49.048	—
	600	33.992	—	49.438	—
	700	41.657	—	49.708	—
	800	48.063	—	49.799	—
	900	53.855	—	49.845	—
	1000	59.277	—	49.890	—

values of 271 K for PuC and 258 K for $PuC_{0.75}O_{0.25}$. The θ_D of PuC (271 K) is consistent with the experimental value of 270 ± 15 K for $PuC_{1.01}$.[40] For $PuC_{0.75}O_{0.25}$, a smaller θ_D indicates a softer lattice and stronger low-frequency phonon vibrations. This is consistent with the additional defect modes caused by oxygen substitution, and it explains the observed increase in low-temperature heat capacity.

3.4 Elastic properties

The elastic properties are evaluated using the "stress–strain technique" based on the applied strains of ±0.002. The stress is determined as a function of the strain, with internal coordinates optimized for each small strain, and the elastic constants are obtained from the derivatives of stress with respect to strain. Because the structures of PuC and $PuC_{0.75}O_{0.25}$ belong to cubic symmetry, there are only three independent elastic constants C_{11}, C_{12} and C_{44}. From the obtained elastic constants, the elastic modulus can be further derived by the Voigt formalism: the shear modulus $G = (C_{11} - C_{12} + 3C_{44})/5$, Young's modulus $Y = 9BG/(G + 3B)$ and Poisson's ratio $\sigma = (B - 2G/3)/(2B + 2G/3)$, where B is the bulk modulus defined by $B = (C_{11} + 2C_{12})/3$. Table 8 lists all elastic constants and associated quantities.

For cubic crystals, the necessary conditions for mechanical stability are given by $(C_{11} - C_{12}) > 0$, $(C_{11} + 2C_{12}) > 0$, $C_{11} > 0$ and $C_{44} > 0$. Our calculated elastic constants satisfy all these conditions, confirming that PuC and $PuC_{0.75}O_{0.25}$ are elastically stable. From Table 8, $PuC_{0.75}O_{0.25}$ exhibits larger G and Y compared to PuC, indicating enhanced hardness. This trend can be explained by the atomic-scale bonding behavior, as shown by Bader charge analysis in Table 2. In PuC, each Pu atom transfers 1.28|e| to the C atom, reflecting the intrinsic ionic character of the Pu–C bond. In $PuC_{0.75}O_{0.25}$, oxygen substitution leads to differentiated charge transfer. Pu atoms near the O atom (Pu_1) lose 1.38|e|, and this is 0.1|e| more than Pu in PuC. The extra charge is transferred to the O atom (Q_B (O) = 7.38e). Pu atoms far from O (Pu_2) retain the same 1.28|e| loss as in PuC, transferred to C atoms. The increased charge transfer for Pu_1 confirms stronger ionic character in Pu–O bonds than in Pu–C bonds. This intensifies electrostatic attraction between ions, strengthens bonding, and leads to higher G and Y values. The fact that only Pu_1 is affected indicates that hardening is localized around oxygen defects, consistent with the moderate difference in elastic moduli. The reliability of our computational approach is supported by the bulk modulus of PuC. Our calculated result of 168.53 GPa is in reasonable agreement with the previously reported value of 172 GPa (SIC-LSD[25]). For $PuC_{0.75}O_{0.25}$, B is slightly lower (160.92 GPa), likely due to local lattice distortion from O substitution. This trend is consistent with Bader volume analysis. Pu_1 in $PuC_{0.75}O_{0.25}$ has a smaller volume (18.66 Å^3) than Pu in PuC (19.77 Å^3). This compression around the oxygen defect may lead to a lower resistance to volume deformation. The G/B criterion can be used to predict the ductile and brittle behavior. According to Pugh's empirical rule,[41] a value higher than the critical G/B ratio of 0.57 is associated with brittleness, while a lower value corresponds to ductility. Our results show that both PuC and $PuC_{0.75}O_{0.25}$ have G/B ratios below 0.57, confirming they are ductile materials. However, PuC is relatively more ductile compared to $PuC_{0.75}O_{0.25}$. This difference is also related to bonding nature. The stronger ionic character of Pu–O bonds restricts atomic slip and thus reduces ductility, whereas the more metallic Pu–C bonding facilitates plastic deformation. The calculated

Table 8 Calculated elastic properties of PuC and $PuC_{0.75}O_{0.25}$ in LSDA + U (U_{eff} = 4.0 eV) framework. G is shear modulus in GPa, Y is Young's modulus in GPa, σ is Poisson's ratio, B is bulk modulus in GPa, and G/B is ratio between shear modulus and bulk modulus

System	C_{11}	C_{12}	C_{44}	G	Y	σ	B	G/B
PuC	225.72	139.94	50.72	47.59	130.49	0.37	168.53	0.28
$PuC_{0.75}O_{0.25}$	228.81	126.97	66.29	60.20	160.56	0.33	160.92	0.37

Poisson's ratios are between 0.25 and 0.45 for typical metals, further supporting their ductile nature.

3.5 Formation energy of O-substituted C defects

The thermodynamic stability for oxygen substituting in PuC is assessed by calculating the defect formation energy (E_{form}) within a $PuC_{0.75}O_{0.25}$ model system. This energy quantifies the energetic cost of replacing a carbon atom with an oxygen atom and reflects the likelihood of defect formation. E_{form} is given by:

$$E_{form} = E_{defective} - E_{perfect} + \mu_C - \mu_O, \quad (6)$$

where $E_{defective}$ and $E_{perfect}$ are the total energies of the supercell with and without the defect, respectively;μ_C and μ_O are the chemical potentials of carbon and oxygen, referenced to graphite and an isolated O_2 molecule. The calculated formation energy is −5.11 eV, indicating that oxygen substitution is a highly spontaneous process. This large energy gain at the atomic scale drives the macroscopic oxidation of PuC. Our result is consistent with the large negative reaction enthalpy of −1000 kJ mol^{-1} (≈ −10.36 eV per formula unit) for $PuC + O_2 \rightarrow PuO_2 + C$.[42] This agreement validates our computational approach and establishes oxygen incorporation as the key first step. The spontaneity originates from the electronic structure of the Pu–O bond. As revealed by our Bader charge analysis, the charge transfer from Pu to O (1.38|*e*|) is greater than that in the Pu–C bond (1.28|*e*|). The stronger ionic character enhances the bond strength, as reflected in the highly negative E_{form}. The large negative formation energy of −5.11 eV demonstrates that PuC is intrinsically unstable towards oxygen ingress. Even under low oxygen partial pressure, thermodynamics strongly favors the dissolution of oxygen into the lattice and the formation of a $PuC_{0.75}O_{0.25}$ solid solution. This atomic-scale finding quantitatively explains PuC's tendency to degrade over time and highlights the necessity of controlling its exposure to the atmosphere.

4. Conclusions

This work reveals the initial stage of plutonium carbide aging by investigating PuC and $PuC_{0.75}O_{0.25}$. We demonstrate that oxygen substitution is thermodynamically inevitable, as evidenced by its large negative formation energy (−5.11 eV). This central result provides the atomic-scale driving force for the degradation process. The oxygen substitution introduces a new peak in the density of states (DOS). The new DOS peak is caused by hybridization between Pu 5f/6d states and O 2p states. Bader charge analysis further demonstrates that Pu ions near the O atom in $PuC_{0.75}O_{0.25}$ are ionized somewhat stronger than those in the PuC system. At the same temperature, the oxygen substitution in PuC causes greater values of H_T–H_{298}, S_T–S_{298}, C_p and C_v relative to pure PuC. Furthermore, the calculated elastic properties reveal that $PuC_{0.75}O_{0.25}$ is anticipated to be harder than PuC, a result consistent with the fact that the Pu–O bond has notably stronger ionic character than the Pu–C bond. Since $PuC_{0.75}O_{0.25}$ is an important corrosion product of plutonium during chemical aging, we expect that our studies on its structure and physical properties can help evaluate the actual performance of plutonium.

Conflicts of interest

There are no conflicts to declare.

Data availability

The data that support the findings of this study are available from the corresponding author upon reasonable request.

Acknowledgements

This work was financially supported by the Natural Science Foundation of Chongqing (Grant No. cstc2021jcyj-msxmX1073).

References

1 D. C. Hoffman, *Advances in Plutonium Chemistry 1967-2000*, American Nuclear Society, 2002.
2 H. G. G. Flores, P. Roussel, D. P. Moore, *et al.*, *Surf. Sci.*, 2011, **605**, 314–320.
3 A. Modin, Y. Yun, M. T. Suzuki, *et al.*, *Phys. Rev. B: Condens. Matter Mater. Phys.*, 2011, **83**, 075113–075120.
4 P. Zhang, B. T. Wang and X. G. Zhao, *Phys. Rev. B: Condens. Matter Mater. Phys.*, 2010, **82**, 144110–144124.
5 H. Nakamura, M. Machida and M. Kato, *Phys. Rev. B: Condens. Matter Mater. Phys.*, 2010, **82**, 155131–155137.
6 J. M. Haschke and T. H. Allen, *J. Alloys Compd.*, 2001, **320**, 58–71.
7 G. Cinader, D. Zamir and Z. Hadari, *Phys. Rev. B*, 1976, **14**, 912–920.
8 M. T. Butterfield, T. Durakiewicz, E. Guziewicz, *et al.*, *Surf. Sci.*, 2004, **571**, 74–82.
9 O. Eriksson, Y. G. Hao, B. R. Cooper, *et al.*, *Phys. Rev. B: Condens. Matter Mater. Phys.*, 1991, **43**, 4590–4597.
10 K. Balasubramanian, T. E. Felter, T. Anklam, *et al.*, *J. Alloys Compd.*, 2007, **444**, 447–452.
11 L. N. Dinh, J. M. Haschke, C. K. Saw, *et al.*, *J. Nucl. Mater.*, 2014, **408**, 171.
12 R. Yang, B. Tang, T. Gao and B. Y. Ao, *J. Nucl. Mater.*, 2016, **473**, 54–60.
13 R. Yang, B. Tang, T. Gao and B. Y. Ao, *Eur. Phys. J. B*, 2017, **90**, 145–154.
14 R. Yang, B. Tang, T. Gao and B. Y. Ao, *Commun. Theor. Phys.*, 2016, **66**, 447–452.
15 L. R. Morss, N. M. Edelstein, and J. Fuger, *The Chemistry of the Actinide and Transactinide Elements*, Dordrecht: Springer, 2006.
16 R. Z. Qiu, J. Tang, J. F. Chen, P. C. Liu and Q. Wang, *Phys. Chem. Chem. Phys.*, 2024, **26**, 14122–14130.
17 C. Ganguly, and D. Vollath, *Quantitative Phase Analysis in the U, Pu-C-System by X-Ray Diffraction*, Karlsruhe, 1974.
18 S. S. Hecker, *Metall. Mater. Trans. A*, 2008, **39A**, 1585–1592.
19 B. Y. Ao, R. Z. Qiu, H. Y. Lu, X. Q. Ye, P. Shi, P. S. Chen and X. L. Wang, *J. Phys. Chem. C*, 2015, **119**, 101–129.

20 X. D. Wen, R. L. Martin, G. E. Scueria, S. P. Rudin and E. R. Batista, *J. Phys. Chem. C*, 2013, **117**, 13122–13142.
21 B. Sun, P. Zhang and X. G. Zhao, *J. Chem. Phys.*, 2008, **128**, 084705–084712.
22 G. Kresse and J. Hafner, *Phys. Rev. B: Condens. Matter Mater. Phys.*, 1993, **47**, 558–561.
23 J. P. Perdew, K. Burke and M. Ernzerhof, *Phys. Rev. Lett.*, 1996, **773**, 865.
24 S. H. Vosko, L. Wilk and M. Nusair, *Can. J. Phys.*, 1980, **58**, 1200–1211.
25 L. Petit, A. Savane, Z. Szotek, W. M. Temmerman and G. M. Stoks, *Phys. Rev. B: Condens. Matter Mater. Phys.*, 2009, **80**, 045124–045132.
26 A. I. Liechtenstein, V. I. Anisimov and J. Zaanen, *Phys. Rev. B: Condens. Matter Mater. Phys.*, 1995, **52**, 5467–5471.
27 U. Benedict, C. Dufour and O. Scholten, *J. Nucl. Mater.*, 1978, **73**, 208–212.
28 J. L. Green, G. P. Arnold, J. A. Leary and N. G. Nereson, *J. Nucl. Mater.*, 1967, **23**, 231–232.
29 J. L. Green, G. P. Arnold, J. A. Leary and N. G. Nereson, *J. Nucl. Mater.*, 1970, **34**, 281–289.
30 T. Gouder, L. Havela, A. B. Shick, F. Huber, F. Wastin and J. Rebizant, *J. Phys.:Condens. Matter*, 2007, **19**, 476201–476212.
31 F. L. Oetting, *The Chemical Thermodynamic Properties of Plutonium Compounds*, The Dow Company, Rochy Flats Division, Golden, Colorado, 1996, pp. 262–297.
32 A. Siegel, K. Parlinski and U. D. Wdowik, *Phys. Rev. B: Condens. Matter Mater. Phys.*, 2006, **74**, 104116–104122.
33 C. Lee and X. Gonze, *Phys. Rev. B: Condens. Matter Mater. Phys.*, 1995, **51**, 8610–8614.
34 S. Limpijumnong and S. Jungthawan, *Phys. Rev. B: Condens. Matter Mater. Phys.*, 2004, **70**, 054104–054108.
35 O. L. Kruger and H. Savage, *J. Chem. Phys.*, 1964, **40**, 3324–3328.
36 S. Baroni, S. de Gironcoli, A. Dal Corso and P. Giannozzi, *Rev. Mod. Phys.*, 2001, **73**, 515–562.
37 C. G. Maier and K. K. Kelley, *J. Am. Chem. Soc.*, 1932, **54**, 3243–3246.
38 R. Wang, S. F. Wang, X. Z. Wu and T. T. Song, *Int. J. Thermophys.*, 2012, **33**, 300–310.
39 A. T. Petit and P. L. Dulong, *Ann. Chem. Phys.*, 1819, **10**, 395.
40 (*a*) *Journée des Actinides*, ed. B. Kanellakopulos and L. Manes, Kernforschungszentrum Karlsruhe GmbH, KfK 2840, EUR 5758 e, 1980; (*b*) J. W. Yang, T. Gao and L. Y. Guo, *Physica B*, 2013, **429**, 119–126.
41 S. F. Pugh, *Philos. Mag.*, 1954, **45**, 823–843.
42 M. H. Rand and T. L. Markin, *Thermodynamics of Nuclear Materials*, International Atomic Energy Agency, Vienna, 1968, p. 637.